Asia-Pacific J. Atmos. Sci., 48(2), 135-143, 2012
DOI:10.1007/s13143-012-0013-7

Line-by-Line Radiative Transfer Model for Infrared Spectrum of AERI

Kwang-Mog Lee[1], Joong-Hyun Park[1], Myoung-Hwan Ahn[2], Mi-Lim Ou[3], and Yoonjae Kim[4]

[1]*Department of Astronomy and Atmospheric Sciences, Kyungpook National University, Daegu, Korea*
[2]*National Meteorological Satellite Center, KMA, Seoul, Korea*
[3]*National Institute of Meteorological Research, KMA, Seoul, Korea*
[4]*Numerical Weather Prediction Center, KMA, Seoul, Korea*

(Manuscript received 10 July 2011; revised 28 November 2011; accepted 9 December 2011)

Abstract: Infrared radiance spectra measured in space or on the ground have been used for many applications, such as the retrieval of atmospheric temperature and humidity profiles. The Korean Meteorological Administration (KMA) recently installed an Atmospheric Emitted Radiance Interferometer (AERI) system at the Korea Global Atmosphere Watch Center (36°32'N, 125°19'E) in Anmyondo to measure the downward radiance spectra on the ground. For further utilization of such interferometeric radiance measurements, an accurate line-by-line radiative transfer model is required. This study introduces a line-by-line radiative transfer model developed at Kyungpook National University (KNU_LBL) and presents comparisons of spectra simulated using the KNU_LBL model and measured by the AERI system, that is installed inside a secure container. When compared with the Atmospheric and Environmental Research (AER) radiative transfer codes, the KNU_LBL model provides nearly identical spectra for various model atmospheres. The simulated spectra are also in good agreement with the AERI spectra for clear sky conditions, and a further improvement is made when taking into account of the emissions and absorption by CO_2 and H_2O for the light path inside the container, even though the path is short.

Key words: Radiative transfer, line-by-line model, AERI, infrared spectrum

1. Introduction

The infrared radiation in the atmosphere originates from both the ground and the atmospheric composition, including clouds, aerosols, and gas molecules. Since infrared radiation contains information on the emitting and absorbing matter, the high resolution spectra observed in space and on the ground have been used to retrieve not only atmospheric temperature and humidity profiles (e.g., Feltz *et al*., 1998, 2003), but also the properties of atmospheric aerosols and clouds (e.g., Sokolik *et al*., 1998; Turner *et al*., 2003; Huang *et al*., 2004; Turner, 2008). In order to exploit such high resolution infrared radiation spectra, the Korea Meteorological Administration (KMA) installed an Atmospheric Emitted Radiance Interferometer (AERI) instrument, developed by the University of Wisconsin Space Science and Engineering Center (Knuteson *et al*., 2004a) and manufactured by Asea Brown Boveri (ABB; Quebec, Canada), in March 2010 at the Korea Global Atmosphere Watch Center (KGAWC, 36°32'N, 125°19'E) in Anmyondo. To secure the instrument, the AERI system is installed inside a container, where the air temperature and humidity are usually different from those outside the container. Although the light path inside the container is not long, neglecting this path could be a source of error for the simulated spectra by the radiative transfer model.

The purposes of present study are to introduce a line-by-line radiative transfer model developed at Kyungpook National University (KNU_LBL) and to simulate the downward radiance spectra measured by the AERI system installed inside a secure container at the KGAWC. The simulated spectra for model atmospheres, such as the U. S. Standard Atmosphere 1976 (US76; U. S. Committee on Extension to the Standard Atmosphere, 1976) and Middle Latitude Summer (MLS) and Middle Latitude Winter (MLW) atmospheres (McClatchey *et al*., 1972), are then compared with those simulated by the Atmospheric and Environmental Research (AER) radiative transfer codes (Clough *et al*., 2005), which are well established and available to the public. The AERI measured spectra are also compared with the simulated spectra by the KNU_LBL model.

2. Model descriptions

The monochromatic downward radiance in the infrared spectral region at the bottom of the atmosphere (BOA) for a clear sky, without any aerosol load, consists of the radiance contributions from the ground to the top of the atmosphere. The downward radiance for a zenith angle of $\theta = \cos^{-1}\mu$ is expressed as follows:

$$I_\nu(\mu) = \int_0^\infty B(T_z)\frac{d\gamma_\nu(\mu)}{dz}dz \quad (1)$$

where $B(T)$ is the Planck function for the temperature T and $\gamma_\nu(\mu)$ is the monochromatic transmittance for the zenith angle μ.

Numerical calculation of the integral transfer equation has been performed for the plane parallel atmosphere, consisting of many homogeneous layers. The temperature variation within an atmospheric layer is assumed to be linear, and the density

Corresponding Author: Kwang-Mog Lee, Department of Astronomy and Atmospheric Sciences, Kyungpook National University, 1370 Sankyuck-dong, Buk-gu, Daegu, Korea.
E-mail: kmlee@knu.ac.kr

weighted averages of the temperature and pressure are defined as the effective temperature and effective pressure of the layer as follows:

$$\overline{T} = \frac{\int_{z_l}^{z_u} n(z)T(z)\,dz}{\int_{z_l}^{z_u} n(z)\,dz}$$
$$\overline{P} = \frac{\int_{z_l}^{z_u} n(z)P(z)\,dz}{\int_{z_l}^{z_u} n(z)\,dz} \quad (2)$$

where z_u and z_l are the altitudes of the upper and lower boundaries of a layer, respectively, and $n(z)$ is the number density of air molecules. The effective temperature and effective pressure define the properties of the homogeneous layer, and are used to calculate optical thickness of the layer.

The contribution of an atmospheric layer to the radiance at the BOA has been calculated by assuming a linear variation of the Planck function with temperature, i.e., $B(T+\delta T) = B(T) + (\partial B/\partial T)\delta T$. When $\partial B/\partial T$ is approximated by $[B(T_u) - B(T_l)]/(T_u - T_l)$, where T_u and T_l are the temperatures at the upper and lower boundaries of the layer, respectively, the contribution calculation results in the same expression as in the linear variation of the Planck function with optical thickness described by Clough *et al.* (1992).

a. Absorption by atmospheric gases

The optical thickness of an atmospheric layer at a given wavelength is calculated by adding the contributions from the nearby absorption lines, called the line-by-line method. The monochromatic optical thickness for a vertical path Δz is calculated as

$$\tau_v = \Delta z \times \left[\sum_i \left\{ \sum_j S_{ji}\, f(v - v_{ji}^0) \right\} n_i + \sigma_v^{cont} n_{cont} \right] \quad (3)$$

where S_{ji} is the line intensity of the j-th line of the i-th atmospheric species, $f(v - v_{ji}^0)$ is the line broadening profile for the line located at v_{ji}^0, n_i is the number density of the i-th species, and $\sigma_v^{cont} n_{cont}$ is the contribution of the continuum spectra. The mixing ratio of a molecular species in an atmospheric layer is defined as the ratio of the column densities of the species and the dry air molecules. This mixing ratio is used to determine the number density of the species.

The absorption line database of HITRAN 2008 (Rothman *et al*., 2009) is used in the present KNU_LBL model, along with the latest version of the water vapor continuum, MT_CKD 2.5 (available from http://www.rtweb.aer.com; Clough *et al*., 2005). The line broadening is calculated using the Voigt profile throughout the altitude range (Drayson, 1976; Wells, 1999). Also included is CO_2 line mixing, which is caused by interference among overlapping lines when inelastic collisions and radiative energy level transition take place (Niro *et al*., 2005; Hartmann *et al*., 2009). Programs provided by Hartmann (personal communication, May 2010) are adopted for the line broadening of the CO_2 absorption band.

b. Vertical grids

In the numerical calculation of the downward radiance at the BOA, the surface is treated as the lower boundary of the lowest atmospheric layer. Starting from the surface pressure, the vertical pressure grids are defined by the following equation:

$$P_l = \left(\frac{x_l - b}{a} \right)^{1/q},\ l = 1, 2, \ldots, N \quad (4)$$

where $a = 1/(p_{sfc}^q - p_{top}^q)$, $b = 1 - a p_{sfc}^q$, $q = 1/3.5$, and $x_l = (l-1)/(N-1)$. In the equation, N is the number of vertical grids, p_{sfc} is the surface pressure, and p_{top} is the pressure of the top grid. Equation (4) results in thin atmospheric layers near the ground and thicker layers as the altitude increases.

The present model uses 81 vertical grids ranging from the surface pressure to 1 hPa, about 50 km, to include the emissions in the stratosphere. However, since most radiosonde data do not extend up to 1 hPa, the atmospheric profiles from model atmospheres, such as US76 (U. S. Committee on Extension to the Standard Atmosphere, 1976), MLS, and MLW (McClatchey *et al*., 1972), are used above the uppermost radiosonde data with a smooth changeover.

3. Comparison with AER model

As a validation of the present KNU_LBL model, the downward radiance spectra for the model atmospheres were calculated and compared with those calculated using the latest version 11.7 of the AER radiative transfer codes (Clough *et al*., 2005). The AER codes are well established and use the same MT_CKD 2.5 for the continuum as the present model. However, the AER codes make use of their own absorption line database based on HITRAN 2004 (Rothman *et al*., 2005) and incorporate an approximated CO_2 line mixing.

For the comparison, the spectra of the downward infrared radiance at the BOA were calculated with a 0.482 cm^{-1} data interval (same as for AERI spectra) for the MLS, MLW, and US76 atmospheres using the AER and KNU_LBL models. Figure 1 shows a comparison of the results. The two spectra calculated using the KNU_LBL and AER models for each model atmosphere are almost identical, indicating that the present model is as accurate as the AER codes. In the case of the MLS atmosphere, where the total precipitable water is 2.40 cm, the radiance differences (Fig. 1d) between the two spectra are negligible. However, for the MLW and US76 atmospheres, where the total precipitable water is 0.68 and 1.16 cm, respectively, small radiance differences are observed in the spectral regions of 500-625 cm^{-1} and 710-800 cm^{-1} (Figs. 1e and 1f). These disagreements are attributed to differences in the H_2O line database and the method of CO_2 line mixing. For instance, the AER data of H_2O lines near 520 cm^{-1} are about 1% larger than those of HITRAN 2008. This results in a radiance difference of about 1% for the US76 atmosphere and

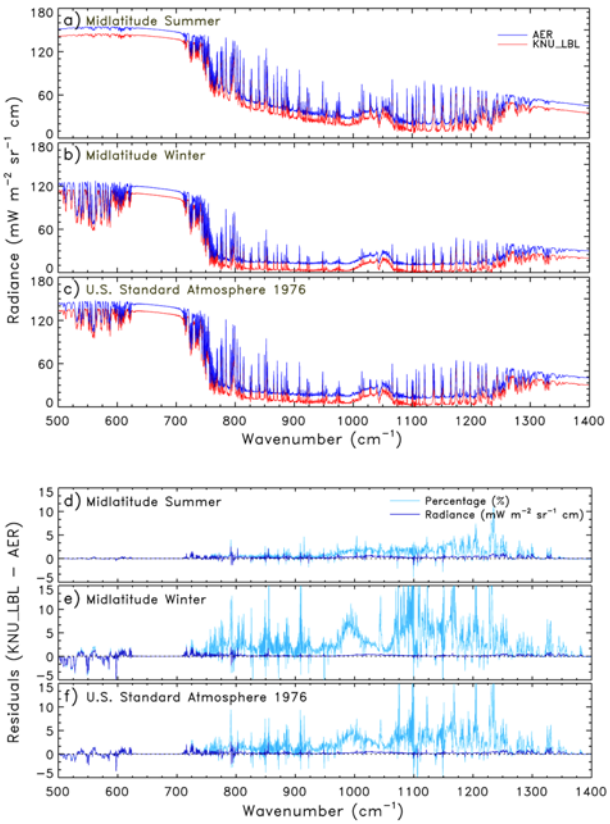

Fig. 1. Comparison of downward infrared radiance spectrum on ground for (a) MLS, (b) MLW, and (c) US76 atmospheres. The AER radiances are shifted up by 10 mW m^{-2} sr^{-1} cm for clarity. The residuals of the spectra calculated from the KNU_LBL and AER models are also shown in (d), (e), and (f), respectively. The blue lines are the radiance residuals, i.e., KNU_LBL - AER (mW m^{-2} sr^{-1} cm), while the sky blue lines are the percentage differences.

about 2% for the MLW atmosphere; similarly, the AER data of H_2O lines near 550 cm^{-1} are about 1.5% larger. The spike near 597 cm^{-1} (see below) for the US76 and MLW atmospheres is caused by the difference in the method of CO_2 line mixing, i.e., excluded in the AER codes.

The effect of the CO_2 line mixing is shown in Fig. 2. The spectrum is calculated using the KNU_LBL model for the US76 atmosphere including CO_2 line mixing and then compared with the spectrum without line mixing (i.e., calculated with the Voigt profile using HITRAN 2008). The resulting effect of the line mixing is to reduce the downward radiance, and the reduction is significant around 620 and 722 cm^{-1}. Note that near 597 cm^{-1}, the line mixing causes a radiance reduction of about 2%.

Figure 3 shows the vertical weighting function calculated for the downward radiance at the BOA for the US76 atmosphere. In the CO_2 band region, most of the radiance contribution is made near the surface, while in the O_3 band region a relatively large contribution is made from the emission in the stratosphere at about 100 hPa. The contributions above 10 hPa are very small throughout the spectral range.

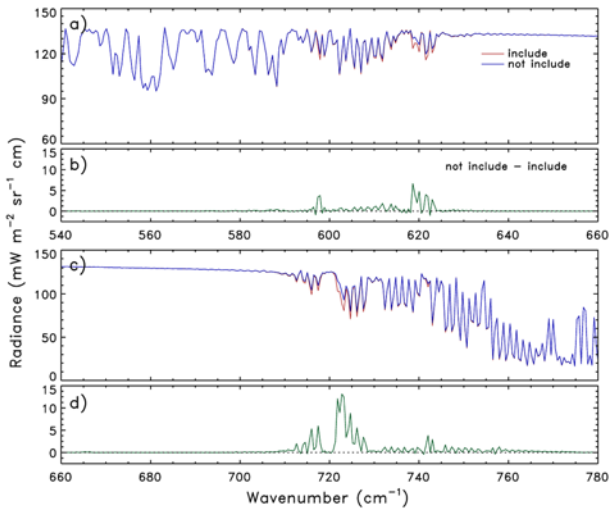

Fig. 2. Effect of CO_2 line mixing from 540 to 780 cm^{-1}. The blue line is the spectrum excluding CO_2 line mixing, while the red line includes the line mixing. A large difference occurred around 722 cm^{-1}.

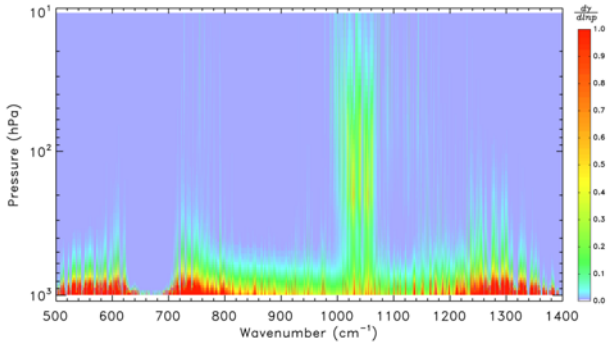

Fig. 3. Weighting function for radiance at bottom of atmosphere. In the CO_2 band, a large contribution is made from the lowest atmospheric layer, while in the O_3 band a relatively large contribution is made from the stratosphere.

4. Simulation of AERI spectra

The AERI system at the Korea Global Atmosphere Watch Center (KGAWC) is operated by the National Institute of Meteorological Research (NIMR, KMA). The instrument design and performance have been described by Knuteson *et al.* (2004a, 2004b). The system is installed inside a secure container, which has a door above the light entrance of the instrument. Figure 4 shows a picture of the system inside the secure container.

The air temperature and humidity inside the container are usually different from those outside. This requires careful modeling of the measured radiance spectra, in particular, for those wavelengths whose weighting function is very large near the ground, even though the light path inside the container is short. Figure 5 shows the air temperature and humidity outside (blue lines), measured by the Automatic Weather Station (AWS), and those inside (red lines) the container, near the AERI selection mirror, from 26 to 27 May 2010. The inside temperature was about 6-15 K warmer than the outside tem-

Fig. 4. AERI system located inside secure container. The light path from the door on the roof to the selection mirror of the AERI system is about 140 cm.

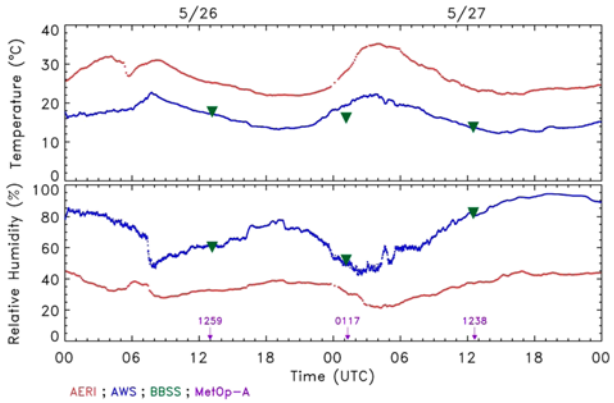

Fig. 5. Air temperature and humidity observed by Automatic Weather Station (AWS) outside (blue line) and inside (red line) container from 26 to 27 May 2010. The green upside-down triangles are the data points of the Graw DFM-09 radiosondes. The arrows at 1259 UTC on 26 May, and 0117 and 1238 UTC on 27 May indicate the times when MetOp-A passed over the KGAWC.

perature, while the relative humidity inside was 15-50% lower than that outside. NIMR launched radiosondes DFM-09 [manufactured by Graw Radiosonde GmbH & Co., KG (Germany)] at 1310 UTC on 26 May 2010 and 0109 UTC and 1231 UTC on 27 May 2010, when the Infrared Atmospheric Sounding Interferometer (IASI) onboard the first satellite of the Meteorological Operational satellite program-A (MetOp-A) passed over the KGAWC, for several purposes including the validation of the IASI Level 2 (L2) products. Thus, vertical profiles of the air temperature and humidity, as well as profiles of greenhouse species, as the products of IASI L2, were available (from http://www.class.ngdc.noaa.gov/saa/products/search?datatype_family=IASI). The arrows along the abscissa in Fig. 5 indicate the times when MetOp-A passed over the KGAWC, and the air temperature and humidity of the radiosondes at the surface level are indicated by green upside-down triangles.

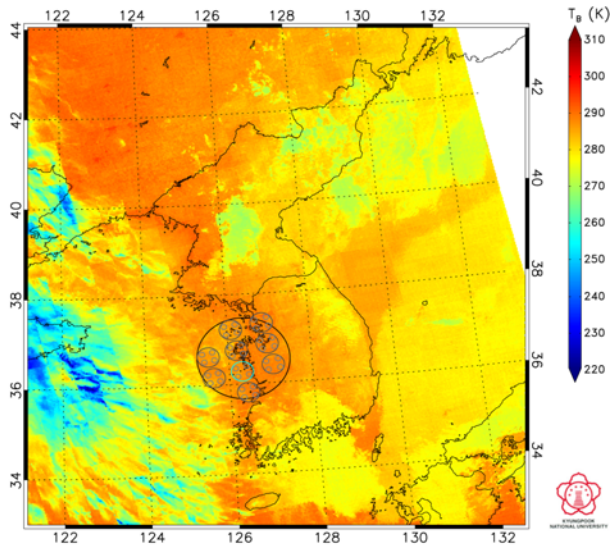

Fig. 6. Ground pixel areas of IASI for orbit 18679 at 1259 UTC on 26 May 2010 around KGAWC. Nine pixels are located within 100 km from the KGAWC (the radius of the large circle centered at the KGAWC is 100 km). The green circle indicates the pixel nearest to the KGAWC. T_B is the brightness temperature of the Integrated Imaging Subsystem (IIS) onboard MetOp-A.

Figure 6 shows the ground pixel areas of the IASI for orbit 18679 at 1259 UTC on 26 May 2010 around the KGAWC. Nine pixels were located within 100 km from the KGAWC (the radius of the large circle centered at the KGAWC is 100 km). The pixel areas of orbit 18687 at 0117 UTC and orbit 18693 at 1238 UTC on 27 May 2010 were very similar to the areas shown in Fig. 6. The IASI L2 temperature and humidity products for the pixels are shown in Fig. 7, along with the profiles of the DFM-09 radiosonde launched at 1310 UTC on 26 May 2010, and 0109 UTC and 1231 UTC on 27 May 2010. The thick lines are the profiles for the pixel area nearest to the KGAWC, indicated by a green circle in Fig. 6. The temperature profiles of the IASI L2 products and the radiosondes were in good agreement up to the uppermost measurement altitude of the radiosondes, except around the tropopause. However, the humidity profiles showed some disagreements. Note the logarithmic scale of the mixing ratios. The fine vertical variations observed by the radiosondes in the middle troposphere were not shown in the IASI L2 profiles. Above the tropopause, the DFM-09 data and IASI L2 products differed significantly from each other. Spaucci *et al.* (2005) previously showed the possibility of large disagreements among humidity measurements from various sensors above the tropopause.

The AERI instrument was operated looking upward to measure the downward spectra. It observed the downward radiance for about 3-4 minutes, collecting 128 interferograms. The spectrum was then calculated from the co-added interferogram through the Fourier transform with the Norton-Beer apodization. Several spectra around 1310 UTC on 26 May remained almost the same, indicating a steady atmospheric

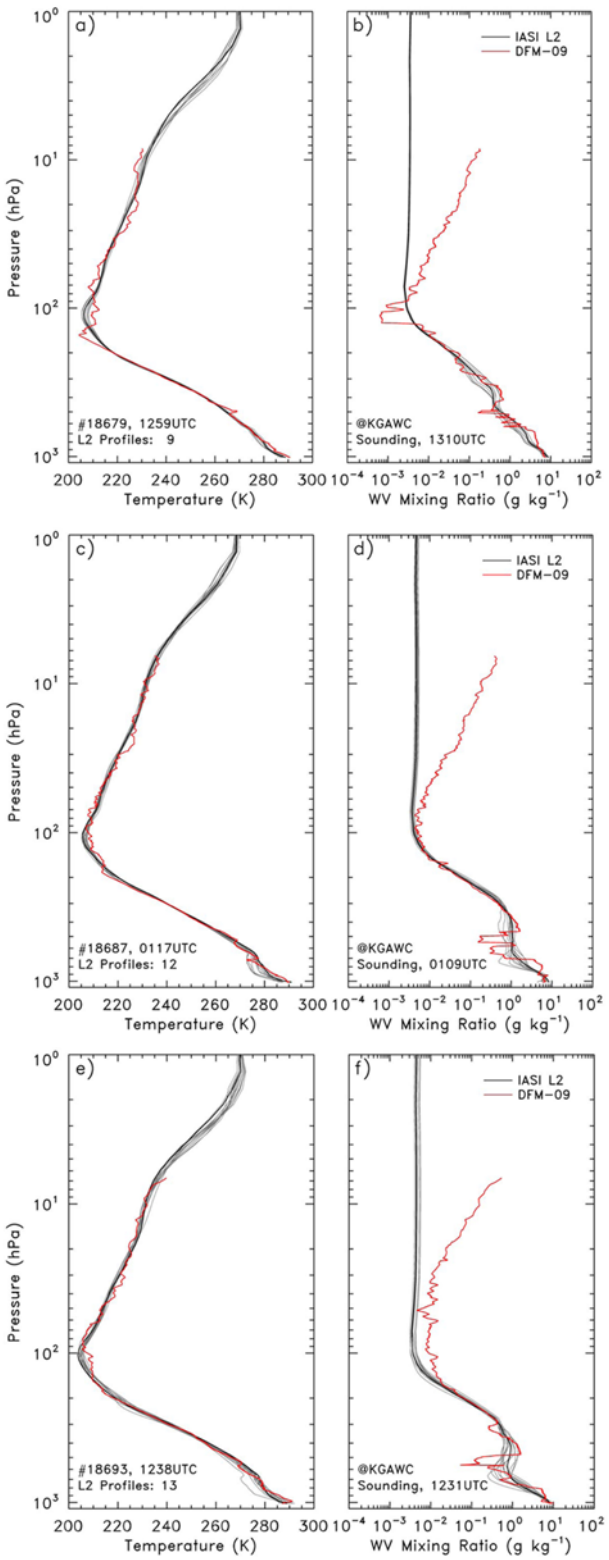

Fig. 7. IASI L2 products of temperature and humidity for ground pixels shown in Fig. 6, along with profiles of Graw DFM-09 radiosondes. The data at 1259 UTC on 26 May 2010 are shown in (a) and (b), the data at 0117 UTC on 27 May 2010 are shown in (c) and (d), and the data at 1238 UTC on 27 May 2010 are shown in (e) and (f). The thick lines are the profiles for the pixel area nearest to the KGAWC, as indicated by the green circle in Fig. 6.

Table 1. The measurement times of the various data used in the simulations.

	26 May	27 May	27 May
AERI	1310 UTC	0125 UTC	1230 UTC
Radiosonde	1310 UTC	0109 UTC	1231 UTC
IASI	1259 UTC	0117 UTC	1238 UTC
Container Temp/Humidity	297.9 K/31%	302.1 K/30%	296.8 K/37%

environment without any cloud interference. In the morning on 27 May, scattered clouds were observed when the radiosonde was launched at 0109 UTC. Around 0125 UTC, i.e., 16 minutes after the launch, a couple of identical spectra were observed without any cloud interference. In the evening on 27 May, the relative humidity at the ground level increased, and was about 82% at 1231 UTC when the radiosonde was launched. At the same time, packs of thin fog passed over the KGAWC (see the high relative humidity in Fig. 5). The downward radiance spectra were simulated for these 3 cases, and Table 1 summarizes the measurement times of the various data used in the simulations.

The simulations were performed for three different temperature and humidity profiles: (1) the radiosonde profiles, assuming constant temperature and humidity above the uppermost measurement level, (2) the IASI L2 profiles for the pixel nearest the KGAWC, shown as the thick lines in Fig. 7, and (3) the combined profiles of the radiosonde and IASI L2 products, i.e., the temperature profile obtained from the radiosonde up to about 10 hPa and the IASI L2 product above 10 hPa, whereas the humidity profile obtained from the IASI L2 product. It is not the intention of this study to find temperature and humidity profiles that give a good agreement between the simulated and measured spectra. The vertical profiles of CO_2, O_3, N_2O, and CH_4 were collected from the IASI L2 products for the pixels, and the mean profiles are shown in Fig. 8, along with the MLS profiles. The mixing ratios of other minor species were adopted from the MLS atmosphere (McClatchey *et al.*, 1972).

The spectra calculations were conducted with a 0.02 cm^{-1} data interval using the KNU_LBL model. To match the resolution of the AERI spectra, the Fourier transform of the spectra was performed to obtain the corresponding interferogram. Then, the inverse Fourier transform of the interferogram with the Norton-Beer apodization was performed to obtain spectra with a 0.482 cm^{-1} data interval. The simulated spectra are compared with the AERI measurements in Figs. 9-11, which show the AERI spectrum and the difference between the measured and simulated spectra, along with the mean difference and root-mean-square difference (RMSD).

Figure 9 shows a comparison of the spectrum at 1310 UTC on 26 May. Our discussion is focused on the temperature and humidity environments, since these are the major sources of disagreement between simulated and measured spectra. A certain degree of disagreement is anticipated in the spectral regions of greenhouse gases, since the gas profiles adopted

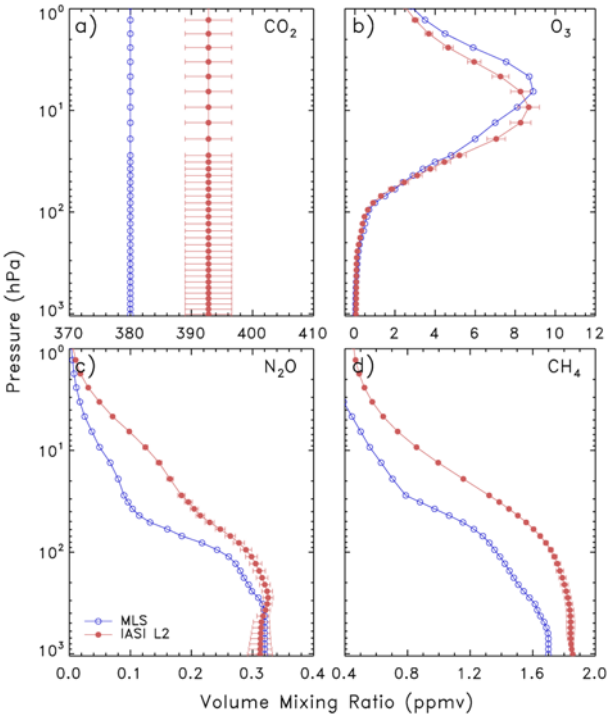

Fig. 8. Mean IASI profiles of CO_2, O_3, N_2O, and CH_4 for ground pixels shown in Fig. 6. The standard deviations of the mixing ratios are indicated by the horizontal bars. The blue lines are the MLS mixing ratios.

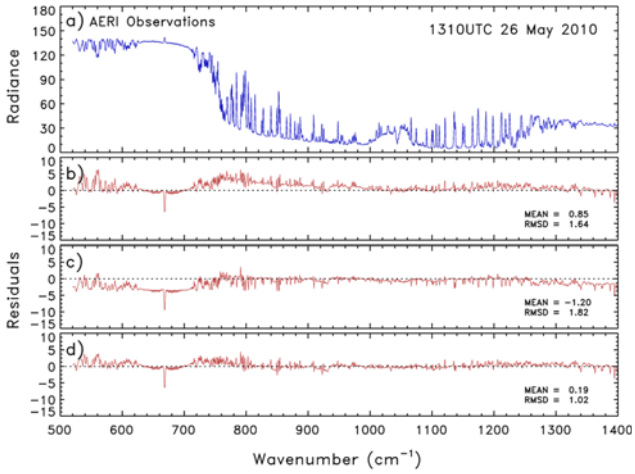

Fig. 9. Downward spectrum measured by AERI instrument and residuals between simulated spectrum using KNU_LBL model and AERI spectrum for 1310 UTC on 26 May 2010. (a) AERI spectrum, (b) residual of radiances, where KNU_LBL spectrum is calculated using radiosonde profiles, (c) residual of radiances, where KNU_LBL spectrum is calculated using IASI L2 profiles, and (d) residual of radiances, where KNU_LBL spectrum is calculated using combined profiles. See the text for descriptions of the radiosonde profiles, IASI L2 profiles, and combined profiles. The radiance and residual units are mW m^{-2} sr^{-1} cm.

from the IASI L2 and MLS atmosphere could be different from those at the AERI measurement times. Figure 9 shows the AERI spectrum and residuals of spectra, i.e., the KNU_LBL

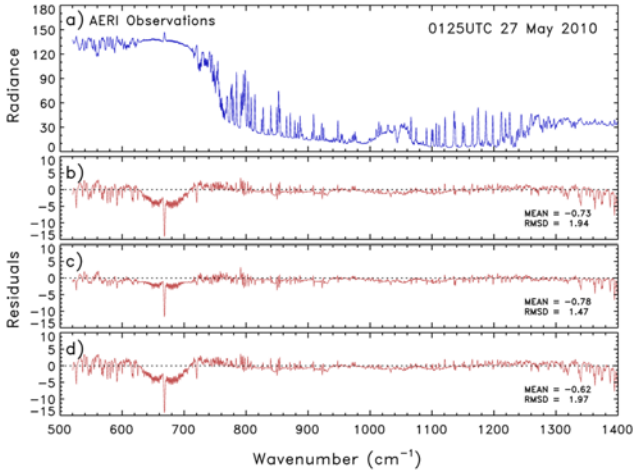

Fig. 10. Same as in Fig. 9, except for 0125 UTC on 27 May 2010.

spectrum - the AERI spectrum, where the KNU_LBL spectrum was calculated using (1) the radiosonde profiles, (2) IASI L2 profiles, and (3) combined profiles described above.

The simulated radiances using the radiosonde profiles, where the precipitable water is 1.78 cm, are larger than the measured values (sky noise level of the AERI for 670-1400 cm^{-1} is smaller than 0.25 mW m^{-2} sr^{-1} cm; Knuteson *et al*., 2004b), in particular, in the H_2O rotational band from 520 to 620 cm^{-1} and window region from 760 to 900 cm^{-1}, where the base line of the radiances are determined by the H_2O continuum. This implies that the humidity profile used in the simulation was different from that when the AERI spectrum was observed. On the other hand, the differences in the CO_2 band are very small, indicating that the temperature profile near the ground was very similar to that at the AERI measurement time. When the IASI L2 profiles (where the precipitable water is 1.57 cm) are used, the simulated spectrum is smaller than the measured value by about 1.20 mW m^{-2} sr^{-1} cm on average for the spectral range of 520-1400 cm^{-1}. However, a large difference of about 4.0 mW m^{-2} sr^{-1} cm occurs in the 620-720 cm^{-1} (CO_2 vibration band) region. At the same time, the simulated spectrum tends to be smaller in the H_2O vibration band at $\nu > 1300$ cm^{-1}. This indicates that the IASI L2 temperatures near the surface were lower than those at the spectrum measurement time. The best agreement with the measured spectrum is obtained when the combined profiles are used. In the spectral ranges of 520-620 cm^{-1} and 720-800 cm^{-1}, differences of about 1.0 mW m^{-2} sr^{-1} cm are observed. These amounts of disagreement are also observed when simulated from the AER codes. A similar magnitude of difference was reported by Turner *et al*. (2004), who used the line-by-line radiative transfer model (LBLRTM) V6.01, an earlier version of the current AER model, to simulate spectra for the 1998-2001 quality measurement experiment data with the precipitable water of 0.0-2.0 cm. Their comparison of the simulated and measured spectra revealed a mean radiance residual of about 0.8 mW m^{-2} sr^{-1} cm for the spectral range of 540-1300 cm^{-1}. However, the spike associated with

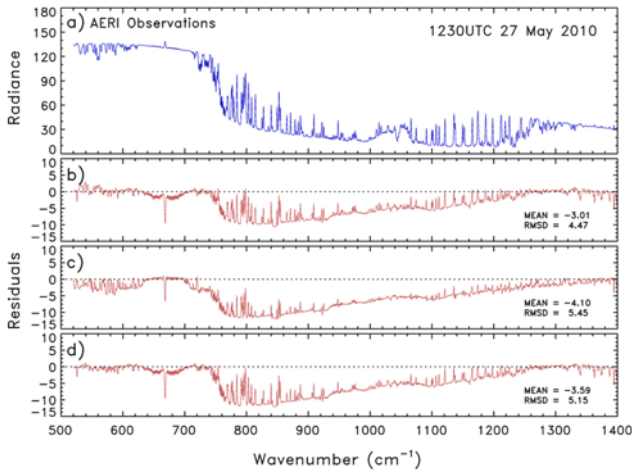

Fig. 11. Same as in Fig. 9, except for 1230 UTC on 27 May 2010. AERI spectrum is contaminated by fog.

the CO_2 Q-branch at 15 μm shown in Fig. 9 is not simulated by both of the KNU_LBL and AER models for any of the three profiles.

In the case of the spectrum at 0125 UTC on 27 May, shown in Fig. 10, the IASI L2 profiles provide the best agreement among the three profiles in terms of the least RMSD value. However, the simulated spectrum in the CO_2 band is smaller by about 2.5 mW m^{-2} sr^{-1} cm than the measured spectrum, indicating that the temperatures near the ground were lower than those at the spectrum measurement time. When the radiosonde profiles (and the combined profiles) are used, the radiance difference in the CO_2 band increases to about 5.0 mW m^{-2} sr^{-1} cm, implying that the radiosonde temperatures near the surface were not correct; as indicated in Fig. 5, the radiosonde temperature at the surface level did not agree with the AWS temperature. Figure 11 shows comparisons of the spectrum at 1230 UTC on 27 May. The simulated spectrum differs significantly from the measured spectrum for all three profiles, especially, in the atmospheric window region. As mentioned earlier, thin fog passed over the KGAWC from time to time for more than 1 hour when the spectrum was measured. Thus, the difference between the measured and simulated spectra appears to be caused by fog contamination.

In order to demonstrate the effects of the short path inside the secure container, having different temperature and humidity environment from outside at the surface pressure level, simulations are performed using the KNU_LBL model for the spectra at 1310 UTC on 26 May and 0125 UTC on 27 May 2010. The path length from the selection mirror of the AERI to the top of the container is about 140 cm. This path is considered as an extra layer underneath the lowest atmospheric layer. The air temperature and relative humidity inside when the spectra were measured are shown in Fig. 5 and summarized in Table 1.

Figure 12 compares the two simulated spectra obtained from the KNU_LBL model, where one spectra includes the light path inside the container (red color), while the other excludes

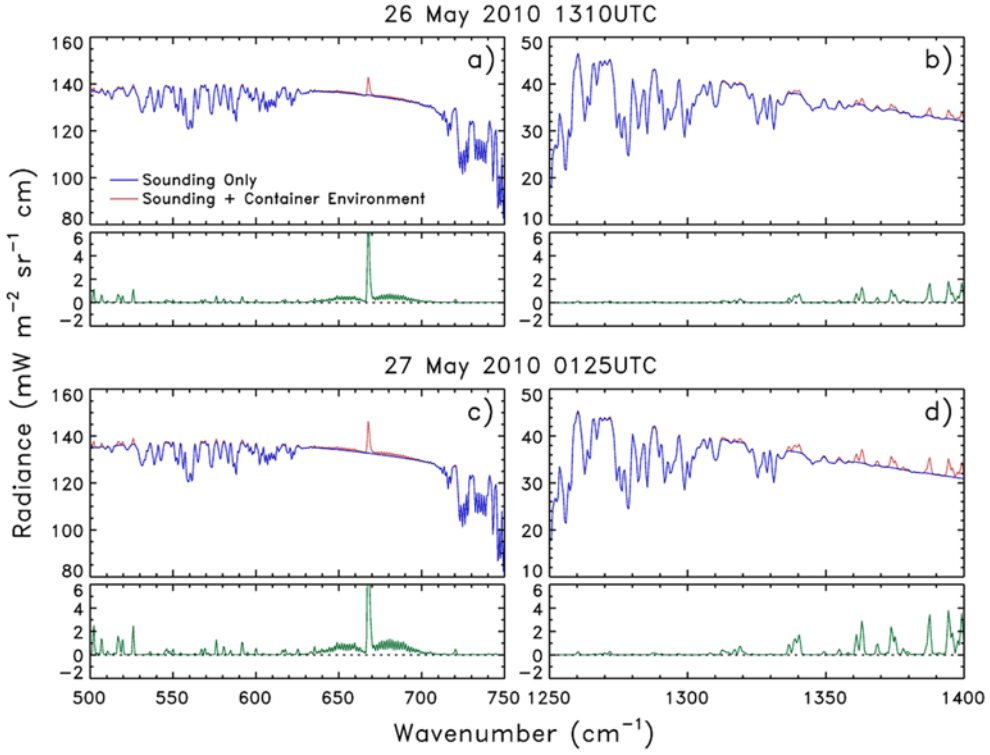

Fig. 12. Effect of air environment inside secure container from 500 to 750 cm^{-1} and from 1250 to 1400 cm^{-1}. The results for 1310 UTC on 26 May 2010 are shown in (a) and (b), and those for 0125 UTC on 27 May 2010 are shown in (c) and (d). The emissions by H_2O and CO_2 at a higher temperature within the container are shown in the lower part of each panel in green.

the light path (blue color). The effects are seen only in the ranges of 500-720 cm^{-1} and 1300-1400 cm^{-1}, which are caused by the emissions from CO_2 and H_2O inside the container at the higher temperatures. In particular, a large emission by the CO_2 Q-branch results in the spike at the center of the band. Since the AERI system is not purged by nitrogen gas, emissions from CO_2 and H_2O in the path from the selection mirror to the beam splitter also contribute to the measured interferogram and resulting radiance. This contribution can be included in a similar way with a different temperature and humidity for the path length. It is assumed that the air environment inside the AERI system is not significantly different from that measured near the selection mirror. However, the results for a total path length from 110 cm to 170 cm do not change significantly. The RMSD value for the range of 520-1400 cm^{-1} decreases from 1.02 to 0.93 mW m^{-2} sr^{-1} cm for 1310 UTC on 26 May, and decreases from 1.47 to 1.13 mW m^{-2} sr^{-1} cm for 0125 UTC on 27 May. Using the AER radiative transfer codes, similar calculations are performed. However, the Q-branch spike is not simulated and the effects are almost negligible compared to those obtained from the KNU_LBL model.

The simulations indicate that even though the path length within the container is short, it is important to include the air environment inside the container in order to simulate the AERI spectra at the KGAWC. Since the radiances in the CO_2 and H_2O spectral regions discussed here are used to retrieve the air temperature and humidity profiles (e.g., Smith *et al*., 1999; Feltz *et al*., 2003), the effects of the light path inside the container have to be taken into account to reduce the errors in the retrieved profiles.

5. Concluding remarks

This study presented a line-by-line radiative transfer model, developed at Kyungpook National University (KNU_LBL), that has flexibility to include a small homogeneous light path, and simulations of the downward radiance spectra measured by the AERI system at the KGAWC installed inside a secure container were discussed. A comparison of simulated spectra calculated from the KNU_LBL model and AER codes (Clough *et al*., 2005) for model atmospheres, such as US76, MLS, and MLW, indicated that the KNU_LBL model is as accurate as the AER codes. The absorption line database and method of CO_2 line mixing of the two transfer models are different, resulting in small disagreements in the corresponding spectral regions.

Ground measurements of the downward radiance spectrum can be used for retrieving the temperature and humidity profiles in the lower troposphere (e.g., Feltz *et al*., 1998, 2003). However, for the AERI system at the KGAWC, the light path inside its secure container has to be taken into account, since simulations of the AERI spectra using the KNU_LBL model are improved when including the environmental conditions inside the container.

The humidity of Graw DFM-09 above the tropopause was much higher than the IASI L2 humidity for the three cases under taken in the present study. The small scale vertical variations in the radiosonde humidity profiles for the middle troposphere were not seen in the IASI L2 profiles. It cannot be concluded that the DFM-09 data are incorrect based on spectra simulations from a limited number of cases. For the spectrum at 1310 UTC on 26 May 2010, however, the simulated spectrum was closer to the measured spectrum when using the IASI L2 humidity.

Acknowledgements. The authors appreciate two anonymous reviewers for providing valuable comments. This study was supported by the project "Research for the Meteorological Observation Technology and Its Application" at the National Institute of Meteorological Research, KMA.

REFERENCES

Clough, S. A., M. J. Iacono, and J.-L. Moncet, 1992: Line-by-line calculations of atmospheric fluxes and cooling rates: Application to water vapor. *J. Geophys. Res.*, **97**, 15761-15785.

_____, M. W. Shephard, E. J. Mlawer, J. S. Delamere, M. J. Iacono, K. Cady-Pereira, S. Boukabara, and P. D. Brown, 2005: Atmospheric radiative transfer modeling: a summary of the AER codes. *J. Quant. Spectrosc. Radiat. Transfer*, **91**, 233-244, doi:10.1016/j.jqsrt.2004.05.058.

Drayson, S. R., 1976: Rapid computation of the Voigt profile. *J. Quant. Spectrosc. Radiat. Transfer*, **16**, 611-614.

Feltz, W. F., W. L. Smith, R. O. Knuteson, H. E. Revercomb, H. M. Woolf, and H. B. Howell, 1998: Meteorological applications of temperature and water vapor retrievals from the ground-based Atmospheric Emitted Radiance Interferometer (AERI). *J. Appl. Meteor.,* **37**, 857-875.

_____, _____, H. B. Howell, R. O. Knuteson, H. Woolf, and H. E. Revercomb, 2003: Near-continuous profiling of temperature, moisture, and atmospheric stability using the Atmospheric Emitted Radiance Interferometer (AERI). *J. Appl. Meteorol.,* **42**, 584-597.

Hartmann, J. -M., H. Tran, and G. C. Toon, 2009: Influence of line mixing on the retrievals of atmospheric CO_2 from spectra in the 1.6 and 2.1 μm regions. *Atmos. Chem. Phys*., **9**, 7303-7312.

Huang, H.-L., W. L. Smith, J. Li, P. Antonelli, X. Wu, R. O. Knuteson, B. Huang, and B. J. Osborne, 2004: Minimum local emissivity variance retrieval of cloud altitude and effective spectral emissivity-simulation and initial verification. *J. Appl. Meteor.*, **43**, 795-809.

Knuteson, R. O., and Coauthors, 2004a: Atmospheric Emitted Radiance Interferometer. Part I: Instrument design. *J. Atmos. Oceanic Technol.,* **21**, 1763-1776.

_____, and Coauthors, 2004b: Atmospheric Emitted Radiance Interferometer. Part II: Instrument performance. *J. Atmos. Oceanic Technol.,* **21**, 1777-1789.

Niro, F., T. Clarmann, K. Jucks, and J.-M. Hartmann, 2005: Spectra calculations in central and wing regions of CO_2 IR bands between 10 and 20 μm. III: atmospheric emission spectra. *J. Quant. Spectrosc. Radiat. Transfer*, **90**, 61-76, doi:10.1016/j.jqsrt.2004.04.005.

McClatchey, R. A., R. W. Fenn, J. E. A. Selby, F. E. Volz, and J. S. Garing, 1972: *Optical properties of the atmosphere.* Rep. AFCRL-72-0497, Air Force Cambridge Res. Lab., Bedford, Mass., USA. 108 pp.

Rothman, L. S., and Coauthors, 2005: The HITRAN 2004 molecular spectroscopic database. *J. Quant. Spectrosc. Radiat. Transfer*, **106**, 139-204.

_____, and Coauthors, 2009: The HITRAN 2008 molecular spectroscopic database. *J. Quant. Spectrosc. Radiat. Transfer*, **110**, 533-572, doi:10.1016/j.jqsrt.2009.02.013.

Sapucci, L. F., L. A. T. Machado, R. B. Da Silveira, G. Fisch, and J. F. G. Monico, 2005: Analysis of relative humidity sensors at the WMO radiosonde intercomparison experiment in Brazil. *J. Atmos. Oceanic Technol.,* **22**, 664-678.

Smith, W. L., W. F. Feltz, R. O. Knuteson, H. E. Revercomb, H. B. Howell, and H. M. Woolf, 1999: The retrieval of planetary boundary layer structure using ground-based infrared spectral radiance measurements. *J. Atmos. Oceanic Technol.,* **16**, 323-333.

Sokolik, I. N., O. B. Toon, and R. W. Bergstrom, 1998: Modeling the radiative characteristics of mineral aerosols at infrared wavelengths. *J. Geophys. Res.,* **103**, 8813-8826.

Turner, D. D., S. A. Ackerman, B. A. Baum, H. E. Revercomb, and P. Yang, 2003: Cloud phase determination using ground-based AERI observations at SHEBA. *J. Appl. Meteorol.,* **42**, 701-715.

_____, and Coauthors, 2004: The QME AERI LBLRTM: A closure experiment for downwelling high spectral resolution infrared radiance. *J. Atmos. Sci.,* **61**, 2657-2675.

_____, 2008: Ground-based infrared retrievals of optical depth, effective radius, and composition of airborne mineral dust above the Sahel. *J. Geophys. Res.*, **113**, D00E03, doi:10.1029/2008JD010054.

U. S. Committee on Extension to the Standard Atmosphere, 1976: *U. S. Standard Atmosphere, 1976*. National Oceanic and Atmospheric Administration, National Aeronautics and Space Administration, United States Air Force, Government Printing Office, Washington, D.C., USA, 227 pp.

Wells, R. J., 1999: Rapid approximation to the Voigt/Faddeeva function and its derivatives. *J. Quant. Spectrosc. Radiat. Transfer*, **62**, 29-48.